Full Text View

Volume 30, Issue 5 (May 2000)

**Journal of Physical Oceanography**
Article: pp. 1099–1110 | Abstract | PDF (491K)

# Winter Circulation and Convection in the Antalya Basin (Eastern Mediterranean)

**Reiner Onken**

*SACLANT Undersea Research Centre, La Spezia, Italy*

**Hüseyin Yüce**

*Department of Navigation, Hydrography and Oceanography, Çubuklu, Istanbul, Turkey*

(Manuscript received July 15, 1998, in final form June 18, 1999)

DOI: 10.1175/1520-0485(2000)030<1099:WCACIT>2.0.CO;2

ABSTRACT

From an oceanographic survey of the Antalya Basin in February 1997 the following horizontal circulation pattern was found: the Asia Minor Current (AMC) was detached from the Turkish coast flowing to the southwest. The Cilician Current was present and feeding the AMC. The AMC exhibited meander wavelengths of about 100 km and phase speed circa 10 cm $s^{-1}$. A train of cyclonic eddies was located at the southern flank of the AMC. The central part of the Antalya Basin was occupied by the Antalya anticyclone. A second anticyclone farther west was identified as the Anaximander anticyclone. From a comparison with previous surveys it is concluded that the circulation of the Antalya Basin is controlled by the position of the AMC. The circulation is cyclonic if the AMC flow path is confined to the coast, and anticyclonic if the path is distant from the coast. In the latter case, the anticyclonic flow may force the Cilician Current to reverse its direction.

A nearly homogeneous pool of Levantine Surface Water was found trapped within the Antalya anticyclone. It is shown that even under light wind conditions, thermohaline convection down to about 200-m depth takes place in this pool. It is speculated that the convectively mixed water body is subject to further transformation by double diffusive mixing with the underlying water and finally contributes to the formation of Levantine Intermediate Water. This is supported by calculations of the necessary double diffusive heat and salt fluxes, which are on the right order of magnitude.

## 1. Introduction

This study is based on a hydrographic survey of the Antalya Basin conducted by the NATO SACLANT Undersea Research Centre in collaboration with the Turkish Navy Department of Navigation, Hydrography and Oceanography in Istanbul. The objective of the survey was to investigate mesoscale circulation pattern in winter and to identify sites of water mass formation.

The Antalya Basin lies in the northern Levantine Basin (Fig. 1), which is part of the Eastern Mediterranean Sea. Until the late 1980s, knowledge of the large-scale horizontal circulation in the upper layers of the Eastern Mediterranean was limited. Considerable progress was achieved by the POEM (Physical Oceanography of the Eastern Mediterranean) surveys 1985–87 (Özsoy et al. 1989; POEM Group 1992; Robinson et al. 1991; Robinson and Golnaraghi 1993). It emerged that modified Atlantic water (MAW) enters the Ionian Basin through the Strait of Sicily as the Atlantic–Ionian Stream (AIS) meanders through the Ionian Basin and then traverses the Levantine Basin as a mid-Mediterranean jet (MMJ) (Fig. 2). The MMJ is accompanied by subbasin-scale anticyclonic and cyclonic recirculation eddies to the south and the north of the jet axis, respectively. The major cyclones are the Rhodes cyclone, southeast of Rhodes and the West Cyprus gyre (WCG), occupying the major part of the Antalya Basin; both cyclones are assumed to be permanent features of the general circulation. At their northern flank, close to the Turkish coast, the latter cyclones are interconnected by the westward flowing Asia Minor Current (AMC), which is fed by the Cilician Current (CC) heading westward between Cyprus and Turkey. In contrast to the AMC, however, the CC is classified as a recurrent or transient feature because it was not verified in all surveys.

Further mesocale analysis of the POEM dataset provided a more detailed description of the Antalya Basin circulation. Özsoy et al. (1989) found an intense anticyclonic eddy dominating the Antalya Basin circulation in October/November 1985. Another anticyclone was found in the 1985 data between the Anaximander Seamounts (Fig. 1) and the Turkish coast [to be referred to as the Anaximander anticyclone (AxAC)]. Anticyclonic eddies, less intense and in slightly different positions, were also identified in the March/April and June 1986 data. Özsoy et al. (1991) show a strong anticyclone covering the western part of the Antalya Basin in June 1987, a feature not present in August/September of the same year, when the entire Antalya Basin exhibits a cyclonic circulation.

In winter, the surface waters of the Eastern Mediterranean are subject to strong transformation processes leading to convection. The convected water mixes with the ambient water and is referred to as Levantine Intermediate Water (LIW) because it is injected into the main thermocline at intermediate depths around 200 m, from where it can be traced throughout the Mediterranean by means of its salinity maximum (Wüst 1961). LIW formation is initialized by favorable atmospheric conditions causing rapid buoyancy loss due to enhanced flux of sensible and latent heat and freshwater. In the Levantine Basin, such conditions occur frequently in winter as a result of strong, cold, dry northerly “poyraz” winds from the Taurus Mountains of Anatolia. According to the recent model study of Lascaratos and Nittis (1998), the primary LIW formation site is the Rhodes gyre, where LIW forms even under climatological conditions. Secondary sites were earlier located by Morcos (1972) in the southern Levantine Basin, in the Aegean Sea (Özturgut 1976; Georgopoulos et al. 1989), and in the Antalya Basin (Özturgut 1976). In the latter study, well-mixed homogenous water bodies with LIW characteristics extending from the surface to depths of about 300 m were found in the center of anticyclones. Other studies also show that LIW trapped in anticyclones is found throughout the Levantine Basin (Özsoy et al. 1986; Hecht et al. 1988; Özsoy et al. 1991; Özsoy and Ünlüata 1993), which is an important aspect in the light of the model results of Wu and Haines (1996), who showed that eddies play a significant role in the redistribution of LIW in the Eastern Mediterranean. However, some of the observations revealed that the water trapped inside the anticyclones is circa 1 K warmer than the LIW according to Wüst’s (1961) definition, and it is unclear whether and how this water contributes to LIW formation.

In this paper, the hydrographic situation of the Antalya Basin is described as derived from the high-resolution survey in February 1997. The horizontal circulation is calculated and compared with those obtained from previous surveys. Recent and earlier observations are summarized in a circulation pattern diagram. An anticyclonic eddy occupying the central part of the basin is investigated in greater detail. A homogenous pool of warm and saline water is trapped in the eddy, and it is shown that this water body is subject to transformation by interaction with the atmosphere. Order of magnitude estimates reveal that the vertical mixing seems to be driven by haline convection, and it is further shown that double diffusion is able to transform the pool to LIW within a reasonable period of time.

## 2. Data and methods

The high-resolution hydrographic survey was conducted by the NATO Research Vessel *Alliance* and the Turkish Vessel *Çubuklu*. The survey consisted of two legs. Leg 1, 8–13 February, was dedicated exclusively to physical oceanography. This leg was again divided into two surveys, 8–11 February (leg 1/1) and 11–13 February (leg 1/2). The purpose of leg 1/1 was to assess large-scale hydrographic conditions, to determine the large-scale circulation pattern, and to identify locations of intermediate depth convection. Leg 1/2 was essentially a repeat survey of leg 1/1 with the intention of investigating temporal changes. The major objectives of leg 2 (16–22 February) were related to acoustics research, which will not be

described, although data from a few oceanographic measurements will be used.

Conductivity–temperature–depth (CTD) casts extending to a maximum depth of 1000 m were obtained from both vessels. The spacing between CTD casts on leg 1 was 20′ (~ 30 km) east–west and 10′ (18.5 km) north–south (Fig. 1). Meteorological observations of air pressure, wind direction and speed, dry and wet-bulb air temperature, and sea surface temperature were carried out from the ship's bridge of *Alliance* every 6 h.

A two-dimensional objective analysis scheme (Bretherton et al. 1976) is used to map irregularly spaced data on a horizontal equally spaced grid, assuming a Gaussian isotropic spatial correlation with length scale $L$ = 50 km, which is of the order of the length scale of the mesoscale features in this region.

## 3. Observational results

### *a. Weather and air–sea fluxes*

Relative humidity, the sum of the fluxes of latent and sensible heat, and the evaporative freshwater flux have been calculated from the directly measured meteorological data. They are, together with the wind speed and direction, illustrated as time series in Fig. 3.

During legs 1/1 and 1/2 the weather was calm with wind speed below 6 m $s^{-1}$. The relative humidity was rather constant between about 40% and 70%. On leg 2 the weather was rougher. The wind speed was considerably higher and reached a maximum value of nearly 16 m $s^{-1}$ on day 22. The relative humidity fluctuates between about 70% and 90% between days 16 and 21 reaching 100% in the morning of day 21 and decreased to about 50% late on day 23.

A poyraz event, characterized by strong and dry northerly winds, forces a rapid buoyancy loss of the near-surface ocean layer due to enhanced release of sensible and latent heat. The above records infer that such an event took place on the last two days of the survey. There, the wind direction rotated from south through east to north, the wind speed increased to its maximum value, and the relative humidity dropped rapidly. The latent and sensible heat flux, which had been less than 160 W $m^{-2}$ between days 8 and 20, increased to nearly 350 W $m^{-2}$ by the end of day 23. At the same time, the evaporative freshwater flux increased from its previous value of about 2 to nearly 11 mm $day^{-1}$. Such large values had only been diagnosed on day 8, caused by the large air–sea temperature difference and low humidity, not by strong winds.

### *b. Horizontal structures*

#### 1) FLOW AND TRANSPORT

Geostrophic currents at 20 dbar were calculated using a level of no motion at 800 dbar and mapped on the regularly spaced grid (Fig. 4, left). The dominating feature of the near-surface flow pattern during leg 1/1 is an anticyclonic eddy in the center of the Antalya Basin—the Antalya anticyclone (AyAC). Its meridional diameter is about 55 km and in zonal direction it extends over about 75 km. Maximum currents of nearly 60 cm $s^{-1}$ are found at its southern flank. The eastern half of a second anticyclone (i.e., the AxAC) with similar meridional extent and strength of flow is visible at the left edge of the figure. The rest of the Antalya Basin is occupied by cyclonic flow. Three cylones, the centers of which are spaced approximately 100 km apart, are aligned along the southern rim of the survey area. Further, three cyclonic flow patterns encircle the AyAC at its northern periphery.

The overall situation found during leg 1/2 is essentially the same, but there are significant changes worth mentioning. The AyAC has changed shape, position, and strength, and the cylonic flow patterns at the southern rim have been shifted in phase. The shape of the AyAC is more elliptic, the center migrated by about 20 km to the southwest (equivalent to a phase speed of nearly 7 cm $s^{-1}$), and maximum velocities are around 40 cm $s^{-1}$. Instead of two cyclonic eddies previously centered at about 30°30′E and 31°20′E, there is only one cyclone at 30°50′E. It is conjectured that this cyclone is identical to the one farther east during leg 1/1, which traveled to the southwest at a mean speed of about 10 cm $s^{-1}$. In the Cilician Basin, there is evidence for the CC meandering westward along the Turkish coast and joined by cyclonic eddies on its southern flank. The flow at the southern flank of the AyAC and AxAC is the AMC, as suggested by Fig. 2. During leg 1/2, there is more indication that this is the approximate flow path.

During leg 1/1, the volume transport (Fig. 4, right) of the AyAC and AxAC is approximately 2 and 4 Sv (Sv $\equiv 10^6$ $m^3$ $s^{-1}$), respectively. The three cyclones at the southern rim of the survey area are weaker, their transport is less than 1.5 Sv, and the transport of the cyclones located to the north and east of the AyAC does not exceed 0.5 Sv. During leg 1/2, the transport of the anticyclones appears to be somewhat weaker, although it it difficult to define the periphery of these eddies

from the contours of the streamfunction. The weak cyclones to the north and the east of the AyAC vanished. The three southern cyclones apparently moved westward, the westernmost one having left the survey area. There is evidence that parts of the cyclone, which is now centered at about (35°25′N, 30°45′E) are drawn northward by the flow around the AyAC and may eventually be advected toward the coast.

2) TEMPERATURE AND SALINITY

The distributions of temperature and salinity are displayed in Figs. 5 and 6. During leg 1/1, the temperature pattern at 10 dbar exhibits high temperatures in the northwestern region of the survey area with local maxima exceeding 18°C. Toward the southeast, temperatures are lower, reaching minimum values of about 16°C in the extreme southwest. Both regions are separated by a well-defined front, the position of which corresponds to the flow of the AMC inferred from Fig. 4. This front will be referred to as the "AMC front." The salinity pattern at the same pressure level is highly correlated with temperature except for a small coastal area in the northeast, where the surface salinity is reduced by fluvial inflow. The highest salinities, exceeding 39.3 psu, are found in the north; toward the southeast, the salinity decreases in the same way as temperature, reaching minimum values less than 39.1 psu in the southwest. During leg 1/2, the near-surface temperature and salinity patterns changed. The most remarkable feature being the change of the position of the temperature–salinity front, which evolved into a northerly meander at about 31°E. This pattern change is consistent with the change of the horizontal flow and transport (Fig. 4), indicating the onshore intrusion of water between the AyAC and the AxAC. In addition, the horizontal area with salinity exceeding 39.3 psu has increased, probably caused by evaporation. Although the horizontal extent of the survey area was comparatively small during leg 2 (not shown), there is clear evidence that the near-surface temperature decreased by some tenths of a degree, which may be due to enhanced net surface cooling and vertical mixing according to fluctuating weather conditions (cf. Fig. 3). Simultaneously, the maximum 10-dbar salinity increased by about 0.02 psu, probably caused by enhanced evaporation.

Except for the location of the front, the temperature and salinity distributions at 10 dbar are only poorly correlated with the patterns diagnosed previously from Fig. 4 because, in the near-surface layers, the dynamical structures are masked by air–sea interaction. In contrast, the patterns at 300 dbar (Fig. 5, Fig. 6, right) are highly correlated in the sense that high and low temperature and salinity correspond to the locations of anticyclonic and cyclonic flow, respectively. Hence, the core of anticyclonic eddies is warm and saline, and lower temperature and salinity prevail in the centers of cyclonic flow patterns.

### *c. Vertical structures*

In order to shed more light on the internal structure of the AyAC, meridional sections of potential temperature and salinity are shown in Fig. 7. CTD casts are spaced 10′ apart, except for leg 1/1 where a cast at 36°N is missing due to malfunctioning of the temperature sensor. Figure 7 clearly reveals that the core of the anticyclone contains a pool of warm and saline water. On leg 1/1, the temperature distribution in the center of the anticyclone represented by cast number 4 is nearly homogeneous between the sea surface and about 300 dbar, the vertical temperature decrease is slightly more than 0.2 K. Qualitatively, the salinity distribution is similar;high and low salinity are correlated with high and low temperature, respectively. The major difference is that temperature decreases monotonically with depth nearly everywhere, whereas the salinity field exhibits interleaving patterns, mainly in the southern half of the section between CTD casts 1 and 4. The vertical scale of the interleaving is of the order of 10 m and the horizontal scale of the order of 10 km. In the same region, both quantities exhibit well-defined vertical step structures with vertical scales of the order of a few tens of meters, indicators of double-diffusive mixing.

As temperature and salinity generally decrease with depth, they have an opposite effect on the rate of change of density. Roughly, an increase of salinity by 0.01 psu is equivalent to lowering the temperature by about 0.04 K. On leg 1 at cast 4 this means that overturning down to about 300 m could be achieved if the surface temperature is decreased by only 0.1 K or by increasing the surface salinity by solely 0.03 psu. Hence, the stratification within the AyAC is potentially unstable with respect to small surface losses of heat and freshwater.

The general situation on leg 1/2 does not differ fundamentally from that of leg 1/1, but there are some changes, which need to be addressed. There is clear evidence that the interior of the anticyclone is warmer on leg 1/2. Comparison with Fig. 5 suggests this to be probably an effect of the translation and change of shape of the anticyclone. In the same way the larger extent of the 39.26 psu isohaline may be explained in terms of horizontal advection; however, this explanation does not obtain for the appearence of the high salinity patch between casts 4 and 6 down to depth 162 m. Here the salinity exceeds 39.3 psu, whereas on leg 1/1 the salinity was lower everywhere within this section. A more careful inspection revealed that on leg 1/1 salinities higher than 39.3 psu were encountered only at one cast in the depth range 0–50 m, whereas on leg 1/2 such high salinities were diagnosed at five casts (cf. Fig. 6). As all these casts were sampled by *Çubuklu* with the same CTD probe, it can be excluded that this is due to different calibration of the *Alliance* and *Çubuklu* probes. Therefore, one must conjecture that the surface density has increased by an amount sufficient to induce vertical overturning of the water column down to 162 m north of the center of the AyAC (cf. Fig. 6). At the same time, the surface salinity must have increased by evaporation. Furthermore, from CTD and XBT (expandable bathythermograph) profiles on February 18 (leg 2),

temperature and salinity were found to be absolutely homogeneous within the top ~ 200 m at about the same location. Thus, it is extremely likely that vertical mixing has continued, leading to further deepening of the warm saline pool.

### *d. Water masses*

According to the water mass definitions published recently by Lermusiaux (1997) (Table 1), MAW was not present in the survey area. This is consistent with Özsoy et al. (1991), who did not find any MAW in this region in winter. Levantine Surface Water (LSW), defined by temperatures above 16.5°C, is found nearly everywhere. In regions of anticyclonic flow LSW attains a vertical extent of more than 250 dbar, and in regions of cyclonic flow the LSW-containing layer is shallower (cf. Fig. 7). The thickness of the LIW layer underlying LSW is between 50 and 100 dbar. It reaches maximum depths of more than 350 dbar in the center of the AyAC and more than 450 dbar in the AxAC. Toward the AMC front and in regions of cyclonic flow it lies closer to the surface. The upper bound of the deepest water mass, LDW, is correlated in the same way with the flow field. Maximum depth values of its upper bound of more than 500 dbar are attained in the center of the AyAC, whereas minimum values around 450 dbar are found in the cyclone centers and close to the coast.

## 4. Discussion and conclusions

### *a. Horizontal circulation patterns*

The key features of the near-surface horizontal flow field in the survey area are the CC, the AMC, the WCG, the AyAC, and the AxAC. Each of these features has been documented in the past, but in many cases, when one was observed, another one was absent. In order to find out which of these features are permanent or recurrent and what relationship might exist between them, Table 2 was constructed to emulate that of Robinson et al. (1991), summarizing all observations by Robinson et al. (1991), Özsoy et al. (1991), Özsoy and Ünlüata (1993), and the present survey.

There is strong evidence for a relationship between the existence of the AyAC and the flow path of the AMC. If the AyAC is present, the AMC is confined to a path about 100 km south. If the AyAC is not present, the AMC flows immediately offshore. A similar relationship appears to exist between the CC and the AxAC. They are present in all surveys except for surveys 2 and 5, giving rise to speculation as to why a "–" in columns 3 and 4 occurs only when "+S" occurs in columns 1 and 2. Thus, there is weak evidence that the AyAC in conjunction with a southern flow path of the AMC are necessary conditions for the disappearance of CC and AxAC.

If survey 4 is ignored, one can identify four different flow patterns I–IV from Table 2, which are sketched in Fig. 8. These patterns reveal that the AMC coincides with the northern rim flow of the WCG (I–IV), which is occasionally fed by the CC (I–III). In pattern I, the WCG extends far north into the Antalya Basin, there is no AyAC, and the CC joins the northwestward cyclonic flow along the coast immediately west of Cyprus. Patterns III and IV are dominated by the AyAC blocking a nearshore northwestward current and forcing the AMC to a flow path south of the AyAC. In III, the CC joins the AMC again; in IV, however, the connection between the AMC and the CC is interrupted, and the CC reverses direction. A characteristic feature of this pattern is that the AyAC covers the entire Antalya Basin extending far to the south. It may be divided into several centers and the AxAC has vanished. A special situation is depicted by II. The AMC is again composed of the northern rim flow of the WCG and the CC, but it is difficult to identify the path of AMC because the entire Antalya Basin is occupied by cyclonic and anticyclonic eddies. Therefore, the notation "SN" was introduced for the second column of the June 1986 survey in Table 2.

The sequence of the sketches I–IV was arranged to provide tentative insight into the life cycle of the Antalya Basin horizontal circulation. Pattern I, defined as the starting point of the cycle, is characterized by a strong nearshore AMC. The AMC starts meandering due to hydrodynamic instability (Özsoy and Ünlüata 1993;Feliks and Ghil 1993) and fills the basin with a few cyclones and anticyclones (II). In a special situation, a large anticyclone may be pinched off from the coastal current to form the AyAC (III). The nearshore flow path of the CC is blocked and if the AyAC is powerful enough, it may even reverse direction (IV). The way, in which the life cycle is closed to resume pattern I, is open to speculation. Due to dissipation, the AyAC surely will weaken and may finally disappear. Another possibility would be that the AMC at the southern rim of the AyAC becomes unstable and that at least parts of the AyAC escape to the south by evolving anticyclonic meanders. This is perhaps the mechanism by which warm and salty anticyclones find their way from the Asia Minor coast into the central Levantine Sea, as postulated by Brenner (1989) and Feliks and Itzikowitz (1987).

### *b. Spatial and temporal variability*

As the horizontal scales of mesoscale variability are expected to be of the order of $2\pi$ times the internal Rossby radius (10–15 km in the northern Levantine Sea), the horizontal resolution of the survey was sufficient to resolve the mesoscale structures. It was found that both the CC and the AMC exhibit meanders with wavelengths of nearly 100 km, which suggests that they are baroclinically unstable. The diameters of fully detached individual eddies are expected to be only half

of that. The only individual eddies covered completely by the survey were the AyAC and two cyclones trapped between the AyAC and the Turkish coast, all exhibiting a diameter between about 40 and 60 km.

As the major portion of the Antalya Basin was surveyed twice within about a week, it was possible to investigate temporal changes. From the displacement of crests and troughs the phase speed of meanders of the AMC and the CC was estimated at 10 cm $s^{-1}$. As from the displacement alone it was not possible to decide whether they travel to the west or to the east, westward propagation was verified by results of a numerical model driven by assimilated data of this survey. It was also possible to show that the AyAC was not stable with respect to its position and shape. The center position was different by about 10–20 km in both surveys, but the center seems to oscillate around a mean position, suggesting that the AyAC is confined to the Antalya Basin and not displaced immediately by the AMC. There is, however, clear evidence that the AyAC interacts strongly with the AMC. Figures 4 and 5 show that it draws in parts of the AMC at its southwestern side and advects them between the AyAC and the Turkish coast. Hence, the AyAC acts as a mixing agent, reducing the contrasts across the AMC front, which may finally lead to its own disappearance.

### *c. Water mass formation*

From Fig. 7 and leg 2 data it was conjectured that air–sea interaction had increased the surface density by an amount that enables convection to about 200-m depth within the period of time of about 10 days. It can be excluded that this mixed layer deepening was solely due to wind mixing because the wind speed was always less than 6 m $s^{-1}$ between 9 and 18 February, and wind mixing alone would not have increased the mixed layer salinity. The following estimate will show that the deepening is probably due to haline convection driven by evaporation. According to Fig. 7, haline-driven overturning to 200-m depth would be enabled by increasing the mean salinity of this layer by about 0.01 psu, which is equivalent to a salt mass of 2 kg. This amount would be released by evaporating 50 mm of water. According to Zavatarelli and Mellor (1995), the monthly climatological freshwater flux in the Eastern Mediterranean in February is about 100 mm $month^{-1}$ (loss) or 33 mm within 10 days, which is at least of the same order of magnitude. The freshwater flux evaluated directly from the meteorological measurements (Fig. 3) yields a mean evaporation rate of about 3 mm $day^{-1}$ amounting also to the same number of about 30 mm within 10 days; thus haline convection is likely.

The estimates reveal that in the Eastern Mediterranean, water mass formation may take place in cyclones (as shown by Lascaratos and Nittis 1998) and in anticyclones. Both induce convection by different types of preconditioning: As doming or outcropping of isopycnals in cyclones induces low vertical stability, surface buoyancy loss leads rapidly to convective overturning, which may extend to great depths in case of large losses. In anticyclones, because of the bowl-shape of isopycnals, the thermocline lies at greater depths and the water pool above is weakly stratified. In this case, surface buoyancy loss leads to further homogenization of the pool and may also deepen the mixed layer; however, mixing to greater depths is prevented by the thermocline. Although in the present survey the homogeneous pool of water in the AyAC was LSW, it may contribute to LIW formation by vertical mixing with the underlying water body. This will lower its temperature and also its salinity toward the LIW temperature–salinity relationship as defined in Table 1. As warm and salty water lies above colder and fresher water, double diffusion is a possible vertical mixing mechanism. From Fig. 7 we have estimated the density ratio

$$R = \frac{\alpha(\Delta T/\Delta z)}{\beta(\Delta S/\Delta z)},$$

where $\alpha \approx 2 \times 10^{-4}$ $K^{-1}$ and $\beta \approx 7.5 \times 10^{-4}$ are the thermal and haline expansion coefficients, respectively, and $\Delta T/\Delta z$, $\Delta S/\Delta z$ the finite difference vertical gradients of temperature and salinity. Using $\Delta T = 1$ K, $\Delta S = 0.15$, and $\Delta z = 20$ m, this yields $R \approx 1.2$ at the bottom of the homogeneous water pool in the center of the AyAC (CTD cast 4); hence rapid growth of salt fingers is extremely likely. Less vigorous growth is expected in other regions of the thermocline where $R$ lies between 2 and 2.7. Now, we shall address the question whether the double diffusive fluxes of salt and heat are capable to convert the trapped water body to LIW within a reasonable period of time. This would require the salinity of the pool to be lowered from ~ 39.25 to LIW salinity of ~ 39.03 and the temperature from ~ 17.8° to ~ 15.4°C (cf. Table 1). Assuming a mean depth of the pool of 100 m, the excess mass of salt to be removed would be $m^e_S \approx 23$ kg and the excess heat $Q^e \approx 1$ MJ. According to Turner (1973) and Stern (1975), the double diffusive buoyancy flux due to salt across an interface with salinity difference $\Delta S$ is

$$\beta F_S = C(gk_T)^{1/3}(\beta\Delta S)^{1/3},$$

where $F_S$ is the salinity flux, $g \approx 9.8$ m $s^{-2}$ the acceleration of gravity, $k_T \approx 1.4 \times 10^{-7}$ $m^2$ $s^{-2}$ the molecular diffusion coefficient for heat, and $C$ a dimensionless function that depends on $R$ only. For $1.2 \leqslant R \leqslant 2.7$, $C$ lies in the range

between 0.1 and 0.06 (Schmitt 1979). For $\Delta S \approx 0.15$ and $C = 0.06$, the buoyancy flux then yields as $\beta F_S \approx 3.7 \times 10^{-9}$ m $s^{-1}$, the salinity flux is $F_S \approx 4 \times 10^{-6}$ m $s^{-1}$, and the vertical flux of salt mass $\hat{F}_S = 10^{-3}\bar{\rho}F_S \approx 5 \times 10^{-6}$ kg $m^{-2}$ $s^{-1}$ using a mean density of $\bar{\rho} \approx 1030$ kg $m^{-3}$. Thus, the timescale to remove the excess salt mass from the pool is $\tau_S = m^e{}_S/\hat{F}_S \approx 53$ days. Repeating the same calculation with the higher value of $C = 0.1$ corresponding to $R = 1.2$, we arrive at a shorter timescale of $\tau_S \approx 32$ days. The double-diffusive heat flux is evaluated from the buoyancy flux ratio

$$\gamma = \frac{\alpha F_T}{\beta F_S}$$

with $F_T$ being the temperature flux. According to Schmitt (1979), $\gamma \approx 0.7$ for $R \leqslant 2.5$; hence $F_T \approx 1.3 \times 10^{-5}$ m $s^{-1}$ for the $C = 0.06$ case. The heat flux yields $Q = \bar{\rho}c_p F_T \approx 53$ W $m^{-2}$ ($c_p \approx 4 \times 10^3$ J $kg^{-1}$ $K^{-1}$ being the specific heat), and the timescale to remove the excess heat is $\tau_Q = Q^e/Q \approx 217$ days. For $C = 0.1$, $\tau_Q \approx 112$ days is obtained. In summary, in the "worst" case the conversion of the homogeneous pool to LIW can be accomplished within about seven months, that is, during the summer and autumn period. As the volume of the pool amounts approximately to $5 \times 10^{11}$ $m^3$, this is equivalent to an annual LIW formation rate of 0.016 Sv—roughly 1% of the total annual LIW formation rate, which is about 1.2 Sv according to the model calculations of Lascaratos and Nittis (1998).

*Acknowledgments*

This work was performed at the SACLANT Undersea Research Centre in La Spezia (Italy). The support of the Turkish Navy Department of Navigation, Hydrography and Oceanography (Istanbul) and the skill and willingness of the crews of NRV *Alliance* and TCG *Çubuklu* are greatly acknowledged. I would like to thank also A. Legner for his help with the drawings.

---

## REFERENCES

Brenner, S., 1989: Structure and evolution of warm core eddies in the Eastern Mediterranean Levantine Basin. *J. Geophys. Res.*, **94** (C9), 12 593–12 602..

Bretherton, F. P., R. E. Davis, and C. B. Fandry, 1976: A technique for objective analysis and design of oceanographic experiments applied to MODE-73. *Deep-Sea Res.*, **23** (7), 559–582..

Feliks, Y., and S. Itzikowitz, 1987: Movement and geographical distribution of anticyclonic eddies in the eastern Levantine Basin. *Deep-Sea Res.*, **34** (9), 1499–1508..

— , and M. Ghil, 1993: Downwelling-front instability and eddy formation in the Eastern Mediterranean. *J. Phys. Oceanogr.*, **23,** 61–78.. Find this article online

Georgopulos, D., A. Theocharis, and G. Zodiatis, 1989: Intermediate water formation in the Cretan Sea (South Aegean Sea). *Oceanol. Acta*, **12** (4), 353–359..

Hecht, A., N. Pinardi, and A. R. Robinson, 1988: Currents, water masses, eddies and jets in the Mediterranean Levantine Basin. *J. Phys. Oceanogr.*, **18,** 1320–1353.. Find this article online

Lascaratos, A., and K. Nittis, 1998: A high-resolution three-dimensional numerical study of intermediate water formation in the Levantine Sea. *J. Geophys. Res.*, **103** (C9), 18 497–18 511..

Lermusiaux, P., 1997: Error subspace data assimilation methods for ocean field estimation. *Harvard Open Ocean Model Reports: Reports in Meteorology and Oceanography*, 55, Harvard University, Cambridge, MA, 402 pp. [Available from Division of Engineering and Applied Sciences, Harvard University, Cambridge, MA 02138.].

Morcos, S. A., 1972: Sources of Mediterranean Intermediate Water in the Levantine Sea. *Studies in Physical Oceanography*, A. L. Gordon, Ed., Vol. 2, Gordon and Breach, 185–206..

Özsoy, E., and Ü. Ünlüata, 1993: Physical oceanography of the Eastern Mediterranean. *Symposium Mediterranean Seas 2000*, N. F. R. Della Croce, Ed., Università di Genova, 207–253..

— ,M. A. Latif, and Ü. Ünlüata, 1986: Mesoscale hydrographic characteristis in the northeastern Mediterranean—November 1985. *UNESCO Rep. Mar. Sci.*, **44,** 75–76..

— ,A. Hecht, and Ü. Ünlüata, 1989: Circulation and hydrography of the Levantine Basin. Results of POEM coordinated experiments 1985–1986. *Progress in Oceanography*, Vol. 22, Pergamon Press, 125–170..

— ,— ,— ,S. Brenner, T. OĞuz, J. Bishop, M. A. Latif, and Z. Rozentraub, 1991: A review of the Levantine Basin circulation and its variability during 1985–1988. *Dyn. Atmos. Oceans*, **15,** 421–456..

Özturgut, E., 1976: The sources and spreading of Levantine Intermediate Water in the Eastern Mediterranean. SACLANTCEN Memo. SM-92, SACLANT ASW Research Centre, La Spezia, Italy, 45 pp..

POEM Group, 1992: General circulation of the Eastern Mediterranean. *Earth Sci. Rev.*, **32,** 285–309..

Robinson, A. R., and M. Golnaraghi, 1993: Circulation and dynamics of the Eastern Mediterranean Sea. *Deep-Sea Res. II*, **40,** 1207–1246..

— ,and Coauthors, 1991: The eastern Mediterranean general circulation: Features, structure and variability. *Dyn. Atmos. Oceans*, **15,** 215–240..

Schmitt, R. W., Jr., 1979: Flux measurements on salt fingers at an interface. *J. Mar. Res.*, **37,** 419–436..

Stern, M. E., 1975: *Ocean Circulation Physics.* Academic Press, 246 pp..

Turner, J. S., 1973: *Buoyancy Effects in Fluids.* University Press, 367 pp..

Wu, P., and K. Haines, 1996: Modeling the dispersal of Levantine Intermediate Water and its role in the Mediterranean deep water formation. *J. Geophys. Res.*, **101** (C3), 6591–6607..

Wüst, G., 1961: On the vertical circulation of the Mediterranean Sea. *J. Geophys. Res.*, **66** (10), 3261–3271..

Zavatarelli, M., and G. L. Mellor, 1995: A numerical study of the Mediterranean Sea circulation. *J. Phys. Oceanogr.*, **25,** 1384–1414.. Find this article online

---

## Tables

Table 1. Water mass definitions in the Levantine Basin according to Lermusiaux (1997). LSW: Levantine Surface Water, MAW: modified Atlantic water, LIW: Levantine Intermediate Water, LDW: Levantine Deep Water.

| Water mass | Temperature range [°C] | Salinity range [psu] |
|---|---|---|
| LSW | ≥16.5 | ≥39.05 |
| MAW | 15.8–17.0 | 38.60–38.80 |
| LIW | 15.0–15.8 | 38.95–39.11 |
| LDW | ≤14.1 | ≤38.87 |

Click on thumbnail for full-sized image.

Table 2. Upper-ocean features of the Antalya Basin. −: not present, +: present, N: flow path along the coast, s: flow path distant from coast, ?: not enough information. Roman numbers in the last column refer to the respective situation depicted in Fig. 8.

| Survey | | AyAC | AMC | CC | AxAC | |
|---|---|---|---|---|---|---|
| 1 | Nov–Dec 85 | + | S | – | + | III |
| 2 | Mar–Apr 86 | + | S | – | – | IV |
| 3 | Jun 86 | + | SN | + | + | II |
| 4 | Mar–Apr 87 | – | N | + | ? | (I) |
| 5 | Jun 87 | + | S | – | – | IV |
| 6 | Aug–Sep 87 | – | N | + | + | I |
| 7 | Jul 88 | – | N | + | + | I |
| 8 | Oct 88 | + | S | + | + | III |
| 9 | Mar 89 | – | N | + | + | I |
| 10 | Aug 90 | – | N | + | + | I |
| 11 | Feb 97 | + | S | + | + | III |

Click on thumbnail for full-sized image.

---

## Figures

Click on thumbnail for full-sized image.

Fig. 1. The Antalya Basin. Water depths are in meters. Positions of CTD casts on legs 1/1 and 1/2 are marked by dots and circles, respectively.

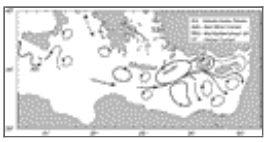

Click on thumbnail for full-sized image.

Fig. 2. Schematic upper ocean circulation of the Eastern Mediterranean (after Robinson et al. 1991).

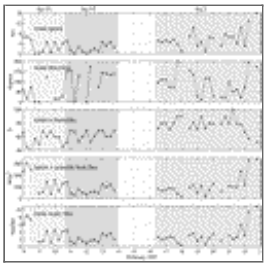

Click on thumbnail for full-sized image.

Fig. 3. Time series of meteorological data and air–sea fluxes.

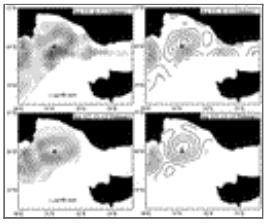

Click on thumbnail for full-sized image.

Fig. 4. Geostrophic currents at 20 dbar (left) and geostrophic volume transport streamfunction (right) between 800 and 20 dbar relative to 800 dbar. The contour interval is 0.5 Sv. The cross serves as a visual aid to track the motion of the center of the AyAC.

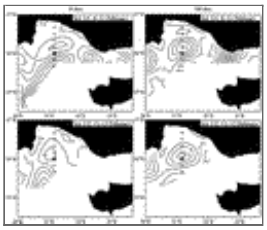

Click on thumbnail for full-sized image.

Fig. 5. Temperature (°C) at 10 dbar (left) and 300 dbar (right). The contour intervals are 0.2 and 0.5 K, respectively. Dots refer to the position of CTD casts of the sections displayed in Fig. 7.

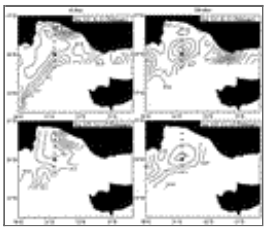

Click on thumbnail for full-sized image.

Fig. 6. Same as in Fig. 5 but for salinity (psu). The contour intervals are 0.02 and 0.05 psu for the left and right panel, respectively.

Click on thumbnail for full-sized image.

Fig. 7. Meridional sections of potential temperature $\theta$ (°C) and salinity S (psu) at 31°10′E for leg 1/1 and leg 1/2. The small numbers above each subplot refer to the positions of CTD casts indicated by dots in Figs. 5 and 6. The contour intervals are 0.2 K and 0.02 psu.

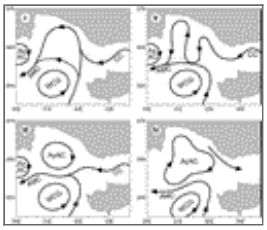

Click on thumbnail for full-sized image.

Fig. 8. Near-surface circulation patterns of the Antalya Basin based on a literature search. Pattern III resembles best the situation of the present survey.

*Corresponding author address:* Dr. Reiner Onken, SACLANT Undersea Research Centre, La Spezia APO AE 09613-5000, Italy.

E-mail: onken@saclantc.nato.int

top